

IFSCC 2025 full paper (IFSCC2025-690)

## ***Bioactive Compound Discovery for Mitochondrial Enhancement and Skin Aging Prevention: A Deep Learning-Aided Screening***

**Jihua Wei<sup>1,\*</sup>, Zhe Feng<sup>1</sup>, Min Yu<sup>2</sup>, Ruiqi Zheng<sup>2</sup>, Minjie Zhang<sup>1</sup>, Yaqi Zhang<sup>1</sup>, Lingling Xuan<sup>1</sup>, Jing Wang<sup>1</sup> and Hu Huang<sup>1</sup>**

<sup>1</sup> Proya Cosmetics Co., Ltd; <sup>2</sup> College of Pharmaceutical Sciences, Zhejiang University, Hangzhou, China

### **1. Introduction**

Mitochondria, the primary cellular organelles, are implicated in both intrinsic and extrinsic skin aging [1]. The skin, an organ with high metabolic activity, relies on mitochondrial ATP production to support the rapid proliferation and turnover of its cells. Notably, age-related mitochondrial dysfunction manifests through distinct phenotypic changes—including fragmentation of mitochondrial networks, loss of membrane potential, and accumulation of mitochondrial DNA mutations—all of which constitute hallmarks of skin aging [2]. These structural and functional changes impair energy metabolism while exacerbating reactive oxygen species (ROS) production, creating a vicious cycle that accelerates cellular senescence in dermal fibroblasts and epidermal keratinocytes [3,4]. Particularly in photoaged skin, ultraviolet (UV) radiation directly damages mitochondrial components, further amplifying oxidative stress and inflammatory responses that degrade extracellular matrix (ECM) integrity [5]. Therefore, pharmacological modulation of mitochondrial function, particularly through bioactive compounds that enhance mitochondrial homeostasis, represents a promising strategy for delaying skin aging.

Conventional screening methods for discovering novel mitochondrial modulators are typically hampered by low efficiency, high expenses, and a focus on single-target assays, potentially missing compounds with diverse effects on mitochondrial homeostasis [6]. High-content screening combined with multiplexed fluorescence imaging offers a powerful alternative by enabling simultaneous quantification of multiple mitochondrial parameters, including morphology, membrane potential, and redox status [7]. Recent advances in deep learning have revolutionized drug discovery by enabling automated feature extraction from complex biological datasets, including cellular images [8]. Deep learning models can identify subtle phenotypic changes induced by bioactive compounds, facilitating the discovery of novel modulators that may not be detected through conventional screening approaches [8]. Therefore, combining high-content screening with deep learning provides an efficient and precise method to discover new mitochondrial modulators that can effectively combat skin aging.

In this study, we developed an innovative deep learning-aided high-content screening platform that combines dynamic mitochondrial imaging with AI-driven predictive modeling to identify

bioactive compounds for mitochondrial enhancement and skin aging prevention. This study integrated high-content imaging of mitochondrial phenotypes in cells subjected to laser-induced ROS damage with a deep learning-based predictive model to prioritize candidate compounds. Candidate compounds were further validated in UVB-induced human dermal fibroblasts (HDFs) to evaluate mitochondrial function and anti-aging effects. Subsequent validation was performed in a novel zebrafish photoaging model, which combines UVB irradiation with tail fin amputation to evaluate tissue regenerative capacity. By combining computational and experimental strategies, this study established a robust framework for discovering novel anti-aging compounds with enhanced efficacy and safety profiles.

## 2. Materials and Methods

### 2.1. Preparation of Compound Combination

Combination Compound 1 (CC-1) comprised 2% spermidine, 0.003% quercetin, 0.51% Mirabilis jalapa extract (MJE), 0.02% vitamin K2 (MK-7), and 0.101% adenosine. Combination Compound 2 (CC-2) comprised 2% spermidine, 0.008% quercetin, 0.51% MJE, 0.02% MK-7, and 0.101% adenosine.

### 2.2. High-Content Imaging and Mitochondrial Dynamic Image Acquisition

For time-resolved imaging, H9c2-MtEGFP cells were seeded in black-walled, transparent bottom 96-well plates at an appropriate density and grown for 24 h before drug treatment. Cells were treated with 10  $\mu$ M spermidine, adenosine, quercetin, or vitamin K2, or 100  $\mu$ g/mL MJE for 24 h before staining. After staining with 20 nM TMRM (Sigma-Aldrich, USA) and 1  $\mu$ g/ml Hoechst 33342 (Invitrogen, USA), cells were automatically imaged in widefield mode using an ImageXpress® Confocal HT.ai High-Content Imaging System (Molecular Devices, USA). A 60 $\times$  air objective lens was used, and one site per well was imaged with DAPI, FITC, and TRITC filters at 10 ms exposure time. Each plate took 1 h to process, with 4-minute image acquisition intervals. The same conditions were used for CC-1 and CC-2. All cell image data were collected by MetaXpress v.6.6 software.

### 2.3. Measurement of Mitochondrial Morphology

HDFs were seeded in 96-well plates for 24 h, pretreated with CC-1 and CC-2 for 24 h, and then irradiated with UVB (1.1 J/cm<sup>2</sup>) before incubated at 37°C in a 5% CO<sub>2</sub> incubator for another 24 h. The fluorescent probe TMRM and Hoechst 33342 were added for 30 min at 37°C, and the fluorescence of Mito-Tracker Red CMXRos was detected to reflect mitochondrial morphology. Images were taken using the ImageXpress® Confocal HT.ai High-Content Imaging System (Molecular Devices, America). Their morphological characteristic parameters were extracted using the image analysis methodology developed by Werner J.H. Koopman's research group [9], implemented in Image Pro Plus 6.0 software to automatically batch-process.

### 2.4. Measurement of ATP Production

HDFs were seeded in 96-well plates for 24 h and pretreated with spermidine, adenosine, MJE, quercetin, MK-7, CC-1 and CC-2 for 24 h. MJE was 100  $\mu$ g/mL, and other compounds were 10  $\mu$ M. Then the cells were irradiated with a UVB dose of 1.1 J/cm<sup>2</sup> and incubated at 37°C in a 5% CO<sub>2</sub> incubator for 24 h. The ATP production of cells was determined by CellTiter-Glo Luminescent Cell Viability assay (Promega, America).

### 2.5. Tricarboxylic Acid (TCA) Cycle Flux

HDFs were seeded in 6-well plates for 24 h and pretreated with CC-1 and CC-2 for 24 h. Then the cells were irradiated with a UVB dose of 1.1 J/cm<sup>2</sup> and incubated at 37°C in a 5% CO<sub>2</sub> incubator for 23 h. The glucose flux through TCA cycle was measured by radiolabeling cells with 2 µCi/ml [6-<sup>14</sup>C]-glucose. Cell suspensions were incubated for 1h in a closed experimental system to trap the <sup>14</sup>CO<sub>2</sub> developed from [<sup>14</sup>C]-glucose. The reaction was stopped by injecting 0.5 ml of 0.8 N HClO<sub>4</sub>. The amount of glucose transformed into CO<sub>2</sub> through the TCA cycle was calculated as described [10].

#### 2.6. Measurement of Mitochondrial Membrane Potential ( $\Delta\psi_m$ )

HDFs were seeded in 96-well plates and pretreated with CC-1 and CC-2 for 24 h. Then the cells were irradiated with a UVB dose of 1.1 J/cm<sup>2</sup> and incubated at 37°C in a 5% CO<sub>2</sub> incubator for 24 h. Mitochondrial membrane potential ( $\Delta\Psi_m$ ) was measured using JC-1 fluorescent probe. The relative  $\Delta\Psi_m$  was quantified as the ratio of red (J-aggregates, 525/590 nm) to green (monomeric form, 490/530 nm) fluorescence intensity, with higher ratios indicating greater polarization. Images were taken and analysed using the ImageXpress® Confocal HT.ai High-Content Imaging System (Molecular Devices, USA).

#### 2.7. Measurement of Cell Senescence

HDFs were fixed and stained using a standard SA-β-gal assay at pH 6.0. After overnight incubation with X-gal solution at 37°C, senescent cells were identified by their characteristic blue staining and quantified by bright-field microscopy.

#### 2.8. Western Blot Analysis

HDFs were lysed and lysates were quantified by performing bicinchoninic acid (BCA) assay. SDS-PAGE was performed and then transferred onto polyvinylidene difluoride membranes. The membrane was incubated with the following primary antibodies: antibody against collagen I and Sirt3. The blots were incubated with horseradish peroxidase-conjugated secondary antibodies. The immunoblots were visualized by enhanced chemiluminescence and exposed on X-ray film. Protein expression was quantified using Image J Program.

#### 2.9. Combined Tail Amputation and UVB Exposure in Zebrafish

Embryos were collected and reared in E3 buffer. At 12 hpf, 200 µM 1-phenyl-2-thiourea (PTU) was added to the medium to suppress melanin synthesis. By 2 dpf, the larvae were divided into the following groups: Control group (Tail amputation only), Model group (Tail amputation + UVB irradiation) and Treatment groups (Tail amputation + UVB + either CC-1 or CC-2), and the UVB irradiation dose was 4 J/cm<sup>2</sup>. Fin regeneration was quantified 24 h post-treatment by neoceratal area measurement.

#### 2.10. Statistical analysis

The data were interpreted as means ± SD. Statistical analysis with one-way analysis of variance (ANOVA) for comparisons among more than two groups were carried out using GraphPad Prism (GraphPad Software, USA). P-values less than 0.05 were considered statistically significant.

### 3. Results

#### 3.1. AI-Aided High-Content Imaging for Screening Mitochondrial Activity Drugs

In our previous study, we developed a high-content screening method based on multiplexed mitochondrial feature labeling [7]. This method utilized dynamic mitochondrial images from

light-induced ROS-damaged H9c2-EGFP cells as cellular phenotypes and combined them with AI algorithms to predict drug activity. The cell model incorporated three fluorescence channels: Hoechst 33342 for nuclear labeling, enhanced green fluorescent protein (EGFP) for mitochondrial morphology, and tetramethylrhodamine methyl ester (TMRM) for mitochondrial membrane potential. Using this AI-based mitochondrial activity prediction method (Figure 1A), we systematically screened 100 natural product monomers and compounds for mitochondrial effects. By comprehensively evaluating two key parameters, "Proportion" (ratio) and "Score" (probability value) (Figure 1B), we identified and ranked the top five potentially active compounds as candidate drugs (hits): quercetin, spermidine, adenosine, MK-7, and MJE (Figure 1C). To validate these candidates, we tested their effects in UVB-damaged HDFs (Figure 1D). All five compounds were found to increase ATP levels in UVB-damaged cells, suggesting potential mitochondrial protective effects.

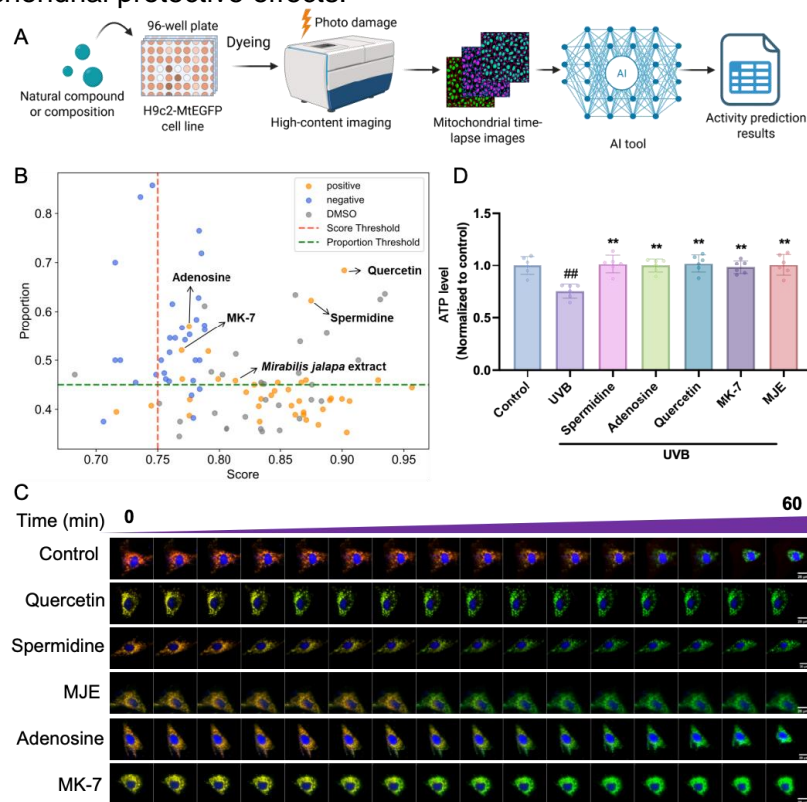


**Figure 1.** Results of deep learning method for predicting mitochondrial activity of drugs. (A) Flowchart for predicting drug activity through mitochondrial dynamics images. H9c2-MtEGFP, rat cardiomyocytes stably labeled with a mitochondrially targeted enhanced green fluorescent protein. (B) Drug screening results. Yellow dots indicate drugs with a predicted label of "positive" (protective), blue dots indicate drugs with a predicted label of "negative" (toxic), and gray dots indicate drugs with a predicted label of "DMSO" (vehicle control). "Score" represents the probability value and sets a threshold of 0.75, and "Proportion" represents the proportion of the number predicted as a label in the cell corresponding to that drug and sets a threshold of 0.45. Dots marked with arrows are the top hits of interest for both Proportion and Score parameters. (C) Single-cell images of mitochondria over time corresponding to the 5 top hits and vehicle control group. Figures are three-channel merged; blue, Hoechst channel; green, MtEGFP channel; red, TMRM channel, scale bar: 20  $\mu$ m. (D) Effects of top 5 hits on ATP levels in UVB-damaged HDF cell model. ##p<0.01 vs Control, \*\*p<0.01 vs UVB.

### 3.2. CC-1 and CC-2 Enhance ATP Production, TCA Flux, and $\Delta\Psi_m$ Stabilization

We further combined these compounds into two formulations (CC-1 and CC-2) and examined their activity in a light-induced ROS-damaged cardiomyocyte model, the mitochondrial phenotypes corresponding to these two combination compounds are shown in Figure 2A. Both CC-1 and CC-2 demonstrated a mitigating effect on cellular shrinkage during the mid-to-late stages of damage. In the UVB-damaged HDF cell model (Figure 2B), both CC-1 and CC-2 significantly increased ATP levels under UVB stress, further indicating their potential mitochondrial protective effects. ATP is generated through both glycolytic and mitochondrial oxidative pathways. To quantify energy metabolism in HDF cells, the culture medium was replaced with [6-<sup>14</sup>C]-glucose-containing medium. Following reaction termination, radioactivity was measured and glucose utilization flux was calculated. As shown in Figure 2C, UVB-irradiated HDFs exhibited a 30% reduction in TCA cycle flux compared to controls. Both CC-1 and CC-2 treatments significantly restored TCA cycle activity to near-normal levels. JC-1 fluorescence probe was employed to monitor  $\Delta\Psi_m$  dynamics. At high membrane potentials, JC-1 forms red-fluorescent J-aggregates within mitochondria, while depolarization shifts emission to green (monomeric form). Figure 2D demonstrates that UVB irradiation induced significant  $\Delta\Psi_m$  dissipation (red/green ratio decreased by 28%,  $p<0.001$  vs control). CC-1 and CC-2 treatments markedly attenuated this effect, maintaining  $\Delta\Psi_m$  at 113% and 93.7% of control levels, respectively ( $p<0.01$  vs UVB group).

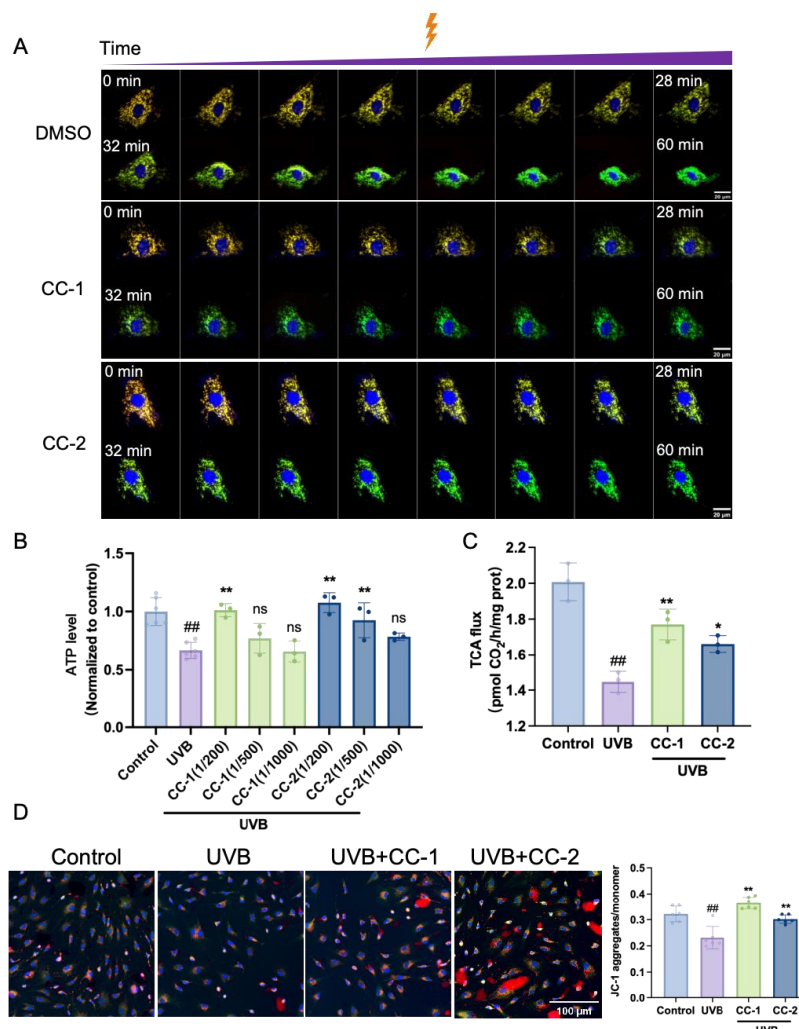


**Figure 2.** Mitochondrial dynamic phenotypes of CC-1 and CC-2. (A) Single-cell images of mitochondria over time corresponding to the DMSO, CC-1 and CC-2. Figures are three-channel merged; blue,

Hoechst channel; green, MtEGFP channel; red, TMRM channel. scale bar: 20  $\mu\text{m}$ . (B-C) Effects of CC-1 and CC-2 on ATP levels and TCA flux in UVB-damaged HDF cell model. (D) JC-1 analysis of mitochondrial membrane potential in HDFs. Fluorescence images (red: J-aggregates; green: monomers) and quantification of red/green ratio, scale bar: 100  $\mu\text{m}$ . ##p<0.01 vs Control, \*p<0.05, \*\*p<0.01 vs UVB.

### 3.3. CC-1 and CC-2 Normalize Mitochondrial Morphometric Parameters

Mitochondria are essential organelles that play pivotal roles in diverse cellular processes, with their functional integrity maintained through a dynamic balance between fusion and fission events. By employing high-content imaging platforms combined with computational morphometric analysis, the Koopman team have systematically quantified mitochondrial phenotypic signatures [9]. UVB-exposed HDFs exhibited severe mitochondrial structural perturbations, including volume contraction, network disassembly and perinuclear clustering (Figure 3A). Both CC-1 and CC-2 treatments effectively preserved mitochondrial ultrastructure. Treated cells exhibited predominantly short, rod-shaped mitochondria with restored network-like structures, evenly distributed throughout the cytoplasm. Quantitative morphometry demonstrated significant recovery of length-related parameters (Perimeter, Roundness) and structural heterogeneity parameter (Heterogeneity), while other measured parameters showing normalization relative to controls (Figure 3B-C).

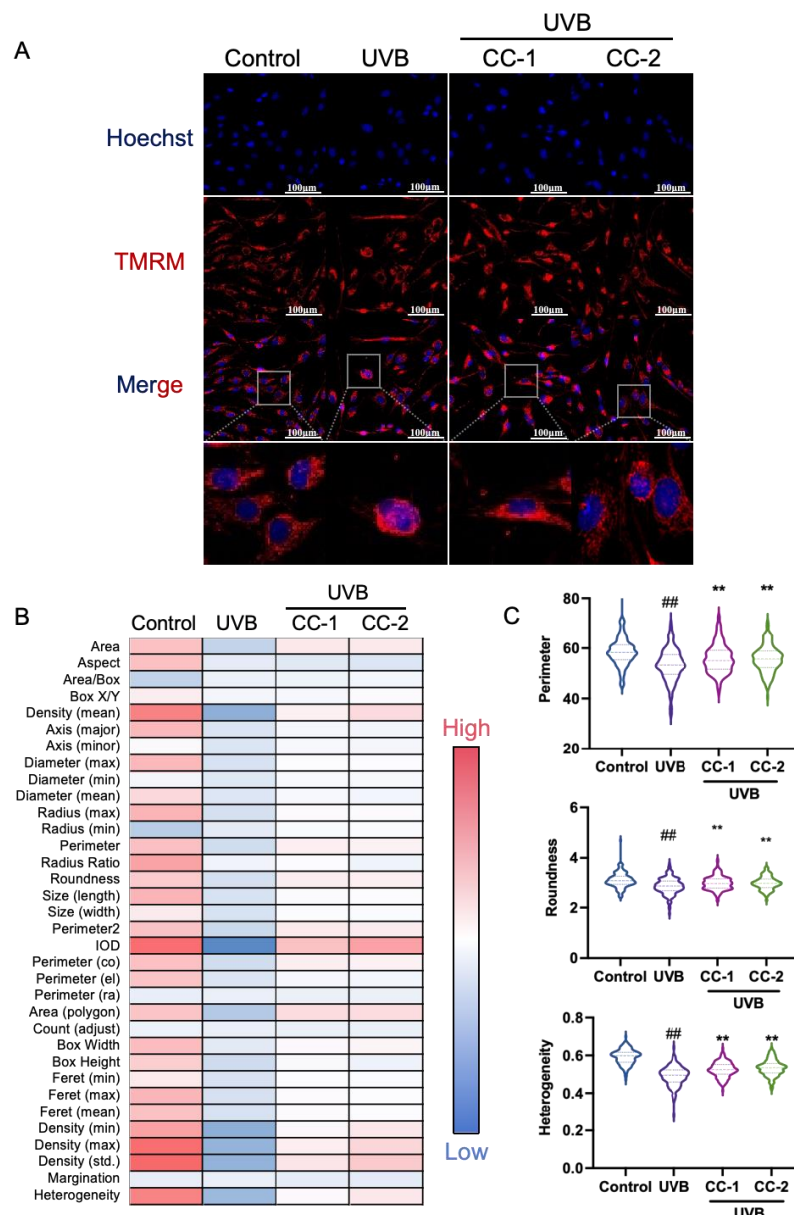


**Figure 3.** CC-1 and CC-2 restore mitochondrial morphofunctional integrity in UVB-exposed HDFs. (A) Representative images of mitochondrial networks stained with MitoTracker Red. Blue, Hoechst channel; red, Mito-Tracker channel. scale bar: 100  $\mu$ m. (B) Clustered heatmap analysis of mitochondrial morphometric parameters. (C) Quantitative assessment of mitochondrial morphological features: Perimeter, Roundness, Heterogeneity. ##p<0.01 vs Control, \*\*p<0.01 vs UVB.

### 3.4. CC-1 and CC-2 Improve Aging-related Phenotype in HDFs and Zebrafish

We then evaluated the effects of candidate formulations CC-1 and CC-2 on UVB-induced skin aging. Using senescence-associated  $\beta$ -galactosidase (SA- $\beta$ -gal), a well-established biomarker of cellular senescence, we found that both CC-1 and CC-2 significantly reduced UVB-triggered SA- $\beta$ -gal accumulation in HDFs (Figure 4A). Compared to UVB exposure alone, both CC-1 and CC-2 treatment upregulated the expression of Collagen I, a key structural protein implicated in skin aging (Figure 4B). CC-1 also enhanced the expression of Sirt3, a longevity-associated protein, suggesting additional anti-aging benefits. The skin structure of zebrafish is similar to that of human skin, consisting of the epidermis, dermis and subcutaneous tissue.

Notably, the zebrafish caudal fin demonstrates exceptional regenerative capacity, making it an ideal model for tissue repair studies. Furthermore, zebrafish have been extensively validated as an *in vivo* oxidative stress model for investigating ultraviolet radiation protection. In this study, we established a tail amputation model coupled with UVB irradiation ( $4 \text{ J/cm}^2$ ) to evaluate the therapeutic potential of test compounds. Drug efficacy was quantified by measuring neoceratal tissue area during fin regeneration, with the experimental workflow illustrated in Figure 4C. As demonstrated in Figures 4D, control group (TA only) exhibited robust fin regeneration within 24 hours post-amputation, while UVB-exposed group (TA+UVB) showed significantly impaired regenerative capacity. Both CC-1 and CC-2 demonstrated therapeutic effects against UVB-induced damage, with CC-2 showing superior efficacy in restoring regeneration.

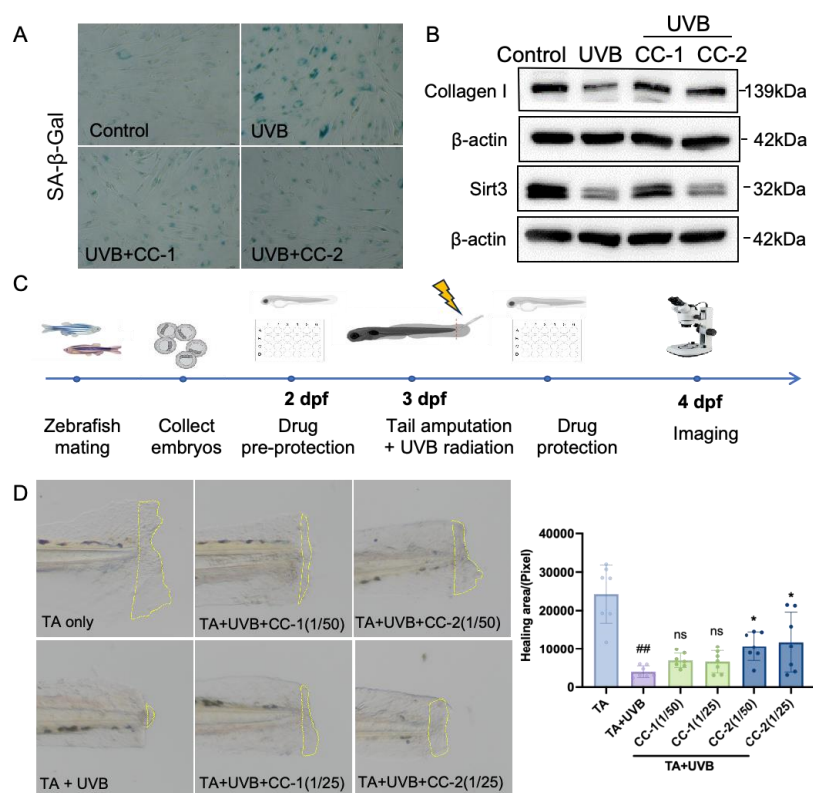


**Figure 4.** CC-1 and CC-2 alleviate the senescence of HDFs and the aging-related phenotype of Zebrafish. (A) Representative images showing SA- $\beta$ -Gal staining in Control, UVB, or CC-treated HDFs. (B) Immunoblots of the protein levels of senescent markers, including Collagen I and Sirt3. (C) Schematic of UVB-injured tail-amputated zebrafish model. (D) Representative images of zebrafish tail regeneration and quantification of the regenerated tail region. Yellow areas indicate newly regenerated tissue. ##p<0.01 vs TA group, \*p<0.05 vs TA+UVB group.

#### 4. Discussion

Our study establishes an innovative deep learning-aided platform for discovering mitochondrial-enhancing compounds, addressing critical limitations in conventional anti-aging drug screening. This platform integrates temporal image feature extraction and large-scale self-supervised pre-training models to achieve intelligent prediction of compounds' mitochondrial protective effects. This approach aligns with recent advances in computational biology, where deep learning has demonstrated exceptional capability to decode complex cellular dynamics from high-content imaging data [7,8]. A key advantage of our platform is its ability to capture

subtle morphological and functional shifts during mitochondrial stress responses, directly addressing the static, "snapshot" limitations of traditional assays [11].

The five identified compounds/natural extracts—spermidine, adenosine, MJE, quercetin, and MK-7—exert protective effects on mitochondrial homeostasis through distinct yet complementary mechanisms. Spermidine, a well-characterized autophagy inducer [12], complements adenosine's role in ATP salvage pathways [13]. Meanwhile, quercetin and MJE exhibit potent ROS-scavenging activities, which help mitigate UVB-induced oxidative stress [14,15]. Recent studies indicate that MK-7, a form of vitamin K2, plays a role in optimizing the mitochondrial electron transport chain [16]. Further investigation revealed that the two composite formulations (CC-1 and CC-2), composed of the above active ingredients, exhibited comprehensive mitochondrial protective effects in UVB-damaged HDFs. Specifically, CC-1 and CC-2 significantly enhanced intracellular ATP production, restored the flux of the TCA cycle, stabilized mitochondrial membrane potential ( $\Delta\Psi_m$ ), and improved mitochondrial morphology.

Our studies further revealed that CC-1 and CC-2 counteract UVB-induced skin aging by reducing cellular senescence and restoring collagen I and Sirt3 expression in HDFs, synergizing with their mitochondrial protective effects. In zebrafish UVB irradiation-caudal fin amputation composite model, both CC-1 and CC-2 demonstrated significant promotion of cutaneous tissue regeneration and repair. These findings provide crucial experimental evidence for developing mitochondria-targeted anti-aging intervention strategies. The zebrafish UVB damage-tail amputation composite model successfully recapitulates key pathological features of skin photoaging, thereby establishing a robust *in vivo* platform for screening potential anti-photoaging compounds.

## 5. Conclusion

This study developed a deep learning-aided platform to screen bioactive compounds for mitochondrial enhancement and skin aging prevention. The identified compounds—spermidine, adenosine, MJE, quercetin, and MK-7—were formulated into two combinations (CC-1 and CC-2), which demonstrated significant mitochondrial protection in UVB-damaged cells by restoring ATP production, TCA cycle flux, and membrane potential. In HDFs and zebrafish, these formulations reduced senescence, promoted collagen synthesis, and accelerated tissue repair. The integration of AI-driven screening with experimental validation offers a powerful approach for developing next-generation anti-aging therapies.

## References

1. Sreedhar, A.; Aguilera-Aguirre, L.; Singh, K.K. Mitochondria in Skin Health, Aging, and Disease. *Cell Death Dis* **2020**, *11*, 444, doi:10.1038/s41419-020-2649-z.
2. Srivastava, S. The Mitochondrial Basis of Aging and Age-Related Disorders. *Genes (Basel)* **2017**, *8*, 398, doi:10.3390/genes8120398.
3. Amorim, J.A.; Coppotelli, G.; Rolo, A.P.; Palmeira, C.M.; Ross, J.M.; Sinclair, D.A. Mitochondrial and Metabolic Dysfunction in Ageing and Age-Related Diseases. *Nat Rev Endocrinol* **2022**, *18*, 243–258, doi:10.1038/s41574-021-00626-7.
4. Jana, B.; Kim, S.; Chae, J.-B.; Chung, H.; Kim, C.; Ryu, J.-H. Mitochondrial Membrane Disrupting Molecules for Selective Killing of Senescent Cells. *Chembiochem* **2021**, *22*, 3391–3397, doi:10.1002/cbic.202100412.

5. Zhang, C.; Gao, X.; Li, M.; Yu, X.; Huang, F.; Wang, Y.; Yan, Y.; Zhang, H.; Shi, Y.; He, X. The Role of Mitochondrial Quality Surveillance in Skin Aging: Focus on Mitochondrial Dynamics, Biogenesis and Mitophagy. *Ageing Research Reviews* **2023**, *87*, 101917, doi:10.1016/j.arr.2023.101917.
6. Arduino, D.M.; Goh, V.; Mokranjac, D.; Perocchi, F. Drug Discovery Assay to Identify Modulators of the Mitochondrial Ca<sup>2+</sup> Uniporter. *Methods Mol Biol* **2021**, *2277*, 69–89, doi:10.1007/978-1-0716-1270-5\_5.
7. Yu, M.; Li, W.; Yu, Y.; Zhao, Y.; Xiao, L.; Lauschke, V.M.; Cheng, Y.; Zhang, X.; Wang, Y. Deep Learning Large-Scale Drug Discovery and Repurposing. *Nat Comput Sci* **2024**, *4*, 600–614, doi:10.1038/s43588-024-00679-4.
8. Pratapa, A.; Doron, M.; Caicedo, J.C. Image-Based Cell Phenotyping with Deep Learning. *Curr Opin Chem Biol* **2021**, *65*, 9–17, doi:10.1016/j.cbpa.2021.04.001.
9. Iannetti, E.F.; Smeitink, J.A.M.; Beyrath, J.; Willems, P.H.G.M.; Koopman, W.J.H. Multiplexed High-Content Analysis of Mitochondrial Morphofunction Using Live-Cell Microscopy. *Nat Protoc* **2016**, *11*, 1693–1710, doi:10.1038/nprot.2016.094.
10. Riganti, C.; Gazzano, E.; Polimeni, M.; Costamagna, C.; Bosia, A.; Ghigo, D. Diphenyleneiodonium Inhibits the Cell Redox Metabolism and Induces Oxidative Stress. *J Biol Chem* **2004**, *279*, 47726–47731, doi:10.1074/jbc.M406314200.
11. Glancy, B. Visualizing Mitochondrial Form and Function within the Cell. *Trends Mol Med* **2020**, *26*, 58–70, doi:10.1016/j.molmed.2019.09.009.
12. Hofer, S.J.; Simon, A.K.; Bergmann, M.; Eisenberg, T.; Kroemer, G.; Madeo, F. Mechanisms of Spermidine-Induced Autophagy and Geroprotection. *Nat Aging* **2022**, *2*, 1112–1129, doi:10.1038/s43587-022-00322-9.
13. Smits, M.A.J.; Schomakers, B.V.; van Weeghel, M.; Wever, E.J.M.; Wüst, R.C.I.; Dijk, F.; Janssens, G.E.; Goddijn, M.; Mastenbroek, S.; Houtkooper, R.H.; et al. Human Ovarian Aging Is Characterized by Oxidative Damage and Mitochondrial Dysfunction. *Hum Reprod* **2023**, *38*, 2208–2220, doi:10.1093/humrep/dead177.
14. Vale, D.L.; Martinez, R.M.; Medeiros, D.C.; da Rocha, C.; Sfeir, N.; Lopez, R.F.V.; Vicentini, F.T.M.C.; Verri, W.A.; Georgetti, S.R.; Baracat, M.M.; et al. A Topical Formulation Containing Quercetin-Loaded Microcapsules Protects against Oxidative and Inflammatory Skin Alterations Triggered by UVB Irradiation: Enhancement of Activity by Microencapsulation. *J Drug Target* **2021**, *29*, 983–997, doi:10.1080/1061186X.2021.1898621.
15. Passari, A.K.; Leo, V.V.; Singh, G.; Samanta, L.; Ram, H.; Siddaiah, C.N.; Hashem, A.; Al-Arjani, A.-B.F.; Alqarawi, A.A.; Fathi Abd Allah, E.; et al. In Vivo Studies of Inoculated Plants and In Vitro Studies Utilizing Methanolic Extracts of Endophytic Streptomyces Sp. Strain DBT34 Obtained from Mirabilis Jalapa L. Exhibit ROS-Scavenging and Other Bioactive Properties. *Int J Mol Sci* **2020**, *21*, 7364, doi:10.3390/ijms21197364.
16. Prasuhn, J.; Kasten, M.; Vos, M.; König, I.R.; Schmid, S.M.; Wilms, B.; Klein, C.; Brüggenmann, N. The Use of Vitamin K2 in Patients With Parkinson's Disease and Mitochondrial Dysfunction (PD-K2): A Theranostic Pilot Study in a Placebo-Controlled Parallel Group Design. *Front. Neurol.* **2021**, *11*, doi:10.3389/fneur.2020.592104.